

PARAMETRIC STUDY AND MITIGATION METHODS FOR WHIRL FLUTTER AFTER OCCURRENCE ON AN ELECTRIC PROPELLER AIRCRAFT

Kyle J. Nelson¹, Christian B. Hoover¹, Jinwei Shen¹

¹The University of Alabama
Tuscaloosa, Alabama 35401 USA
kjnelson2@crimson.ua.edu
cbhoover@crimson.ua.edu
jinwei.shen@eng.ua.edu

Keywords: Aeroelasticity, Whirl Flutter, Multibody Dynamics

1 INTRODUCTION

NASA is developing an all electric aircraft aimed to be three times more efficient than the internal combustion aircraft it is based on. The Scalable Convergent Electric Propulsion Technology and Operations Research (SCEPTOR) vehicle aimed to fit these desires is the X-57 Maxwell [1]. The aircraft is a derivative of an Italian built light aircraft dubbed the Tecnam P2006T. Whereas the Tecnam is a dual turboprop aircraft, the X-57 is an all electric vehicle with a unique propulsion system. The propulsion system fitted to the X-57 is made of 14 total propellers along the entire span of the aircraft, including two main drive rotors and 12 smaller rotors fitted along the rest of the span. The main drive rotors will be used during all phases of flight, while the smaller inboard rotors are used exclusively during the take-off and landing phases of flight [2]. The X-57's long, slender wings have a high aspect ratio and experience stall conditions during take-off and landing phases of flight [3]. The small inboard rotors will provide the downwash over the wing needed to prevent stall conditions. Development of the aircraft is broken into three modifications of the original Tecnam aircraft. The version of the aircraft being tested is the third mod of the aircraft, while the second mod of the aircraft is an altered Tecnam P2006T with the internal combustion engines replaced with electric motors [4]. The fourth mod is the aircraft with fourteen total rotors, twelve being mounted along the span of the wing, and two main drive rotors mounted to the wing tips [4].

Propeller whirl flutter was discovered analytically by Taylor and Browne [5]. Whirl flutter became a topic of discussion during the 1960s after two Electra aircraft crashed [6]. After the crash, it was determined that weakened pylon stiffness from a damaged mount allowed the aeroelastic instability, whirl flutter, to occur. For a propeller mounted non-rigidly, the "whirling" motion is a self-sustained motion about the unperturbed position of the rotor. These two crashes prompted study on propeller whirl flutter with a scale model of an Electra aircraft in the NASA Langley's Transonic Dynamics Tunnel [7]. Consequently the Electra studies set the precedent for researchers to include proprotor aircraft in whirl flutter studies. Fortunately, a similar whirl flutter related incident did not occur for roughly 30 years. Unfortunately, an undetected crack on a Beech craft airplane incurred whirl flutter to occur and fatally destroyed the aircraft in the 1990's. Records from the Beechcraft incident showed that the pilot was calm and acting normal until the crash happened. This implies that the onset of the propeller whirl flutter and the resulting destruction was a swift and violent occurrence.

The X-57 Maxwell aircraft is meant to be physically piloted, therefore the ability to identify and reverse whirl flutter upon onset is crucial. Whirl flutter is an ever present danger that must be considered in the development of propeller driven aircrafts. This paper will discuss a multibody dynamics simulation approach to identify the whirl flutter boundary for the system. This paper will also discuss the steps taken to model pilot inputs in response to the flutter as a mitigation or reversal method to dampen out the "whirling" motion. Taking into consideration the abhorrent results of the Electra and Beechcraft crashes, techniques to mitigate or reverse propeller whirl flutter are crucial for increasing the survivability of the aircraft. Through modeling, the determination of the flutter point in a variety of flight conditions gives a low cost option to physical testing that could result in destructive results. Furthermore, computational modeling of the aircraft allows researchers to subject the aircraft to a variety of conditions with greater repeatably.

2 ANALYTICAL MODELS

The conceptual drawing and key variables of the tip propeller for the X-57 Maxwell aircraft are shown in Figure 1 and Table 1. For the investigation of whirl flutter stability, a semi-span structural model is developed to calculate the frequencies and damping ratios of the wing symmetric modes.



Figure 1: Concept of X-57 Maxwell, Image From NASA

Table 1: Key Aircraft Parameters

Property	Value
Number of Propellers	14
Tip Prop Number of Blades	3
Tip Prop Diameter (ft)	5
Take-Off RPM	2700
Cruise RPM	2250
Cruise Speed (kts)	150
Wing Semi-Span (ft)	14
Wing Nominal Chord (ft)	2.1

2.1 Analytical Models of X-57 Maxwell

Dymore is a finite element (FE) based multibody dynamics code for the comprehensive modeling of nonlinear flexible multibody systems [8]. Derived in an inertial Cartesian frame, the equilibrium equations and constraints are set up using the Lagrange multiplier method. This approach forms a set of differential-algebraic equations that are then solved using a robust time integration scheme. The element library in Dymore includes rigid and deformable bodies as well as joint elements. The deformable bodies are set up using the FE method with the beams and shells modeled as geometrically exact. The aerodynamic forces in Dymore are computed either by using a built-in lifting line theory or through external aerodynamic code coupling.

The Dymore model of the X-57 Maxwell aircraft is shown in Figure 3. The model includes the wing, pylons, tip propellers, and the masses for the small inboard propellers. The wing and propeller blades are modeled as beams. The development of the wing and propeller blades are shown in detail in the two previous studies [9, 10]. The inboard propellers, pylon, and nacelle of the large tip propellers are constructed as rigid body masses with their appropriate inertial properties. The propeller blade pitch bearings are modeled using revolutes joints. The

pylon mount pitch and yaw flexibility are captured with tuned linear springs. The aerodynamic forces acting on the X-57 are modeled using both quasi-steady and unsteady lifting line theories developed by Peters [11]. In addition, the propeller inflow is determined by using a three-dimensional nonlinear dynamic inflow model using three inflow states. A lookup table is used to define the aerodynamic coefficients on the propeller blades and wing. The aerodynamic interaction between the propeller and wing is ignored.

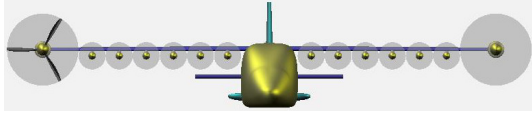


Figure 2: X-57 Maxwell Illustration, Image From NASA

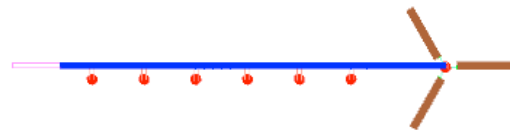


Figure 3: Dymore X-57 Maxwell Semi-Span Model

2.2 Modified X-57 Wing

Since the X-57 is specifically designed to not encounter propeller whirl flutter inside the design envelope [9], the structural model has to be modified to introduce flutter to study flutter mitigation methods. For this study, the pylon springs were reduced in stiffness while the wing properties were left as is. The reduction in pylon stiffness dropped the pylon frequencies and caused two second out-of-plane bending modes to appear, one coupled with both the pylon pitch and the other with the pylon yaw motion. A comparison of the original X-57 modes and frequencies to the modified X-57 is given in Tables 2 and 3.

Table 2: Original X-57

Mode	Frequency (Hz)
Out-of-Plane	2.389
In-Plane	7.033
Second Out-of-Plane	15.192
Torsion	16.784

Table 3: Modified X-57

Mode	Frequency (Hz)
Out-of-Plane	2.379
In-Plane	7.014
Second Out-of-Plane with Pylon Yaw	14.817
Second Out-of-Plane with Pylon Pitch	15.147
Torsion	16.235

2.3 Whirl Flutter

Dymore uses the Prony method to identify the wing damping based on the wing transient response [12, 13]. For this study, a baseline whirl flutter mode is identified and used to evaluate different methods of reducing or reversing the instability. The wing modes are perturbed at each individual mode's natural frequency and the transient response recorded. The transient wing and pylon motion are analyzed using a prony analysis where the frequencies and damping ratios of the system are identified.

3 ANALYTICAL RESULTS

3.1 Parametric Study on Pylon Stiffness

The parametric study looks at the effect of reducing the pylon stiffness springs that allow the propeller/pylon system to pitch and yaw. For this study, the ratio of pylon pitch to yaw spring stiffness was kept constant at 0.54. Only a reduction in pylon stiffness was considered as increasing the pylon springs would only increase the stability margin as shown in a previous study [10]. Figure 4 and Table 4 show the change in frequency per mode due to a reduction in

Table 4: Frequency (Hz) for each Model Based on % Pylon Stiffness

Mode	100	75	50	25	20	18	15	12	10	5
1	2.39	2.39	2.39	2.38	2.38	2.38	2.38	2.38	2.37	2.36
2	7.03	7.03	7.03	7.02	7.02	7.02	7.02	7.01	7.00	6.92
3	15.19	15.18	15.16	15.07	15.02	14.99	14.88	13.74	12.61	9.10
4	16.78	16.75	16.67	16.47	16.37	16.31	15.35	14.85	14.71	13.81
5	33.88	30.74	26.25	19.40	17.52	16.70	16.25	16.14	16.05	15.78
6	37.28	37.20	37.12	36.92	36.82	36.76	36.64	36.45	36.25	34.82
7	49.27	49.09	48.74	47.70	47.18	46.90	46.35	45.57	44.85	42.02
8	58.29	57.85	56.72	55.64	55.44	55.36	55.24	55.12	55.05	54.86
9	59.39	58.43	58.18	57.76	57.59	57.50	57.34	57.12	56.94	56.28

pylon stiffness. The stiffness spacing is due to there being a point of interest around 15% of the nominal pylon stiffness. There is a large spread over the frequencies of mode five and a similar spread at mode three. Interestingly enough, modes three and four are the ones that go unstable as shown later in the paper.

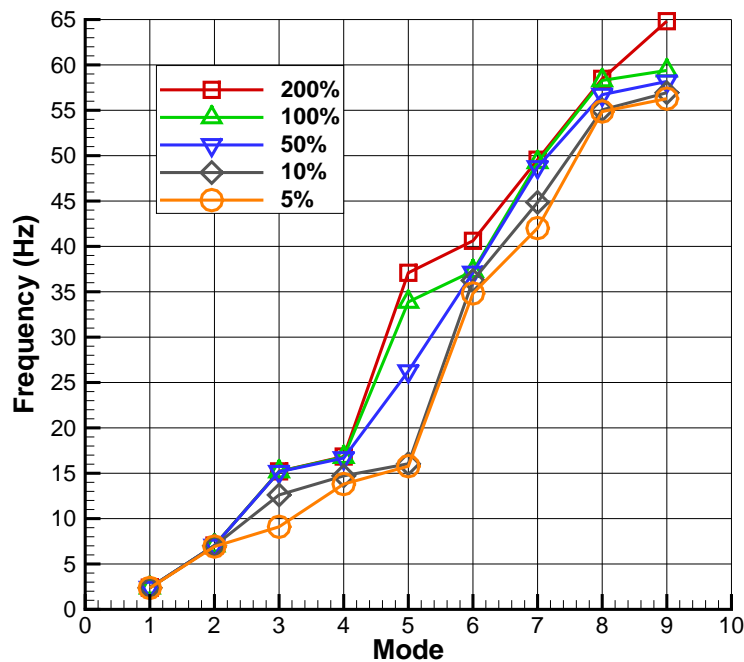


Figure 4: Order of Modes Per Pylon Stiffness in Order of Ascending Mode

The baseline values for frequency and damping ratios for a nominal pylon stiffness are shown in Figures 5 and 6. These figures show that over the flight speeds tested, the semi-span system is stable. Modes 7 and 8 do decrease as the flight speed increases, but none the less, remain stable.

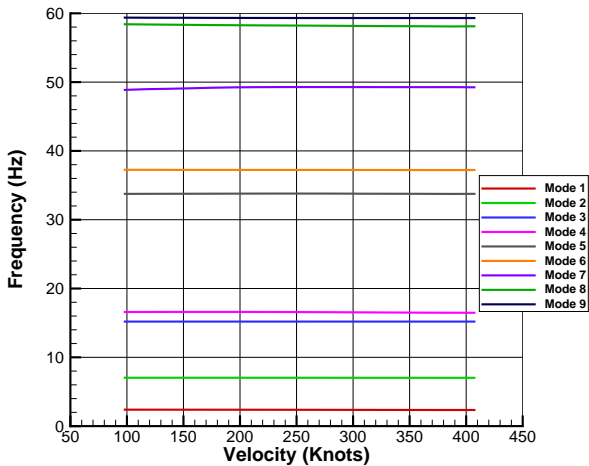


Figure 5: Baseline Frequencies

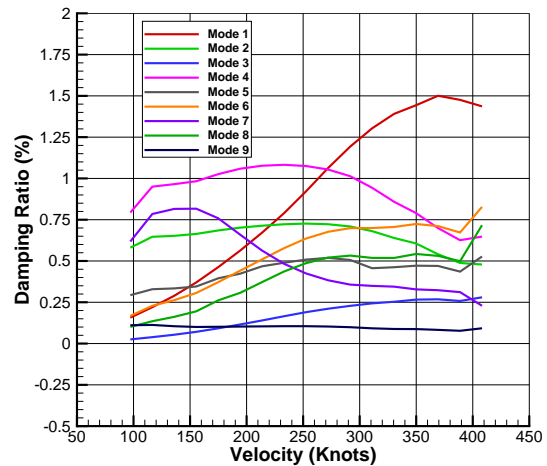


Figure 6: Baseline Damping Ratios

The previous parametric study [10], showed that a pylon stiffness of 15% of the nominal, caused the semi-span system to go unstable. Figures 7 and 8, show the frequencies and damping ratios of the system with this reduced pylon stiffness. The frequency of mode 5 decreases considerably from the baseline test in Figure 5, while the damping ratios change for each mode. With the pylon stiffness equal to 15% of the nominal stiffness, mode 4 becomes unstable around 350 knots, over 2 times the planned cruise speed of the aircraft.

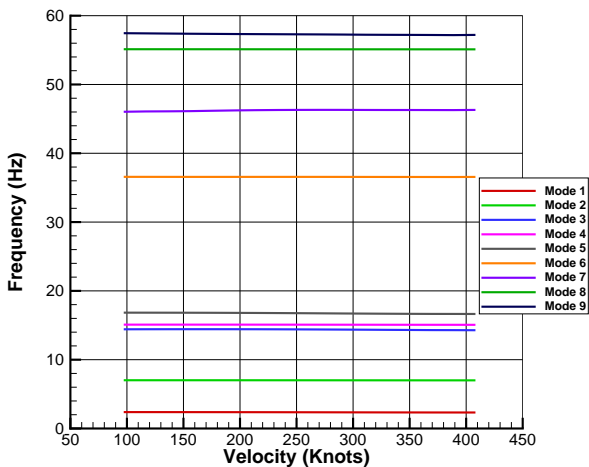


Figure 7: 15% Pylon Stiffness Frequencies

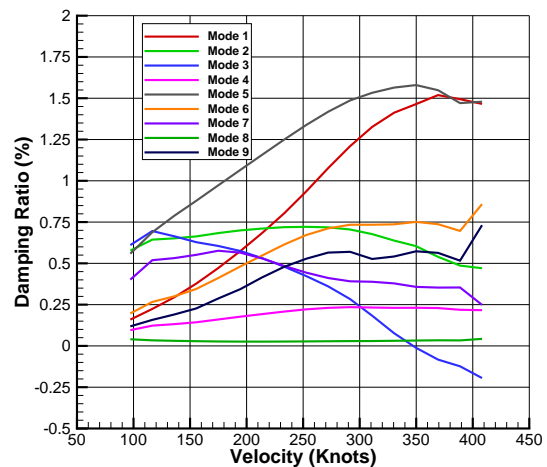


Figure 8: 15% Pylon Stiffness Damping Ratios

3.2 Addition of Wing Aerodynamics

Figures 5 through 8 show the frequency and damping ratios for the semi-span model without wing aerodynamics to examine the effect of just the rotor aerodynamics. Wing aerodynamics add additional aerodynamic damping to the system, so it is typically stabilizing. The following section will detail results that contain wing aerodynamics as well as without wing aerodynamics. Once again, the baseline frequency and damping ratios of the system need to be established, which are detailed in Figures 9 and 10. In these figures, the semi-span system is stable across the vast flight speed range that was tested. All of the modes see an increase in damping ratios with the addition of wing aerodynamics when compared to the system without (Fig 6).

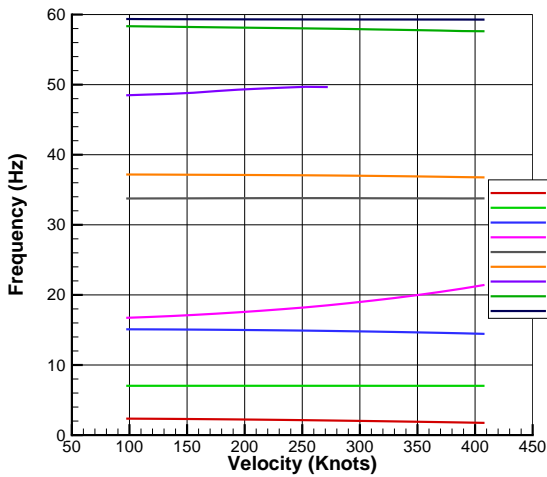


Figure 9: Baseline Frequencies with Wing Aerodynamics

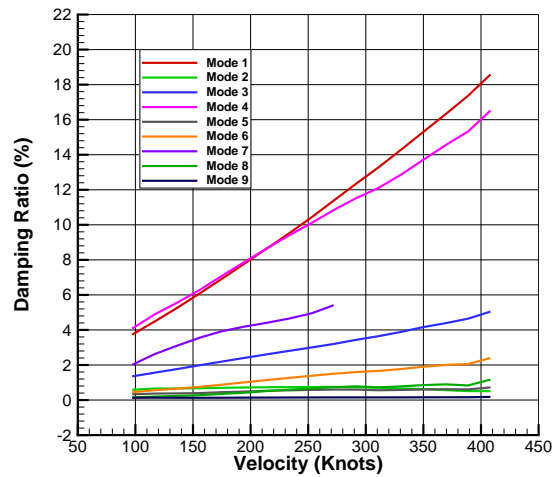


Figure 10: Baseline Damping Ratios with Wing Aerodynamics

Previous results have shown that a weakened pylon spring will allow the pylon pitch and yaw motions to become unstable. The instability is shown in Figure 8. Expanding the range of pylon spring stiffness to plus and minus 3% of that crucial 15% stiffness case with wing aerodynamics is shown in the following figures.

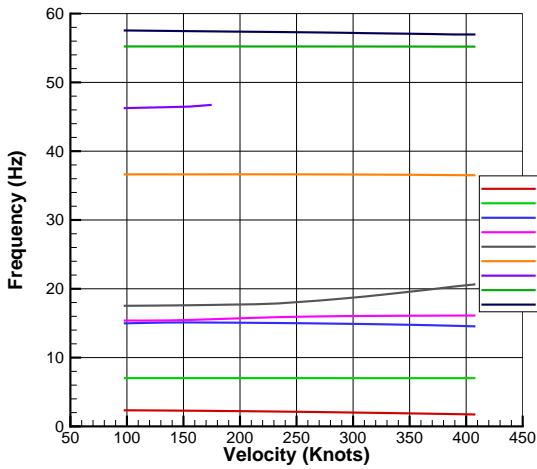


Figure 11: 18% Pylon Stiffness Frequencies with Wing Aerodynamics

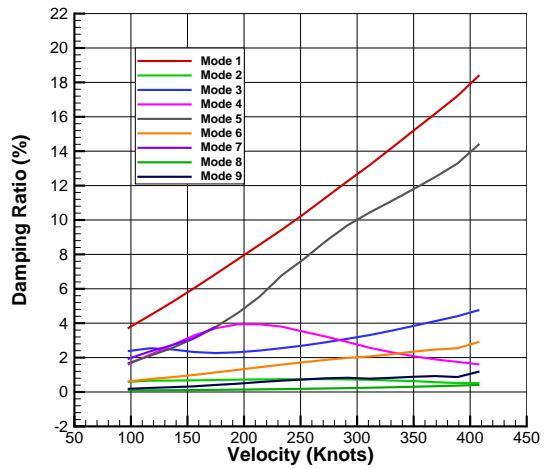


Figure 12: 18% Pylon Stiffness Damping Ratios with Wing Aerodynamics

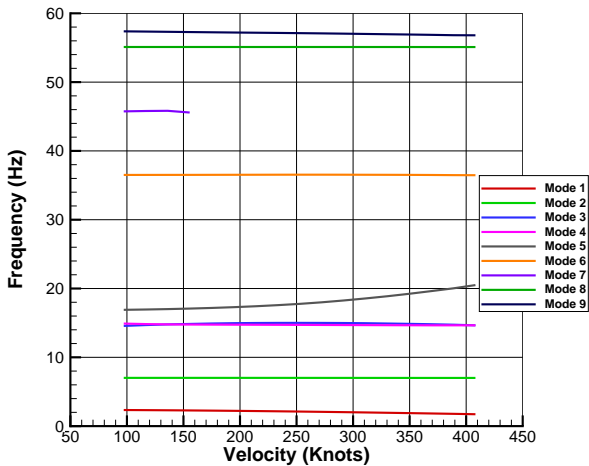


Figure 13: 15% Pylon Stiffness Frequencies with Wing Aerodynamics

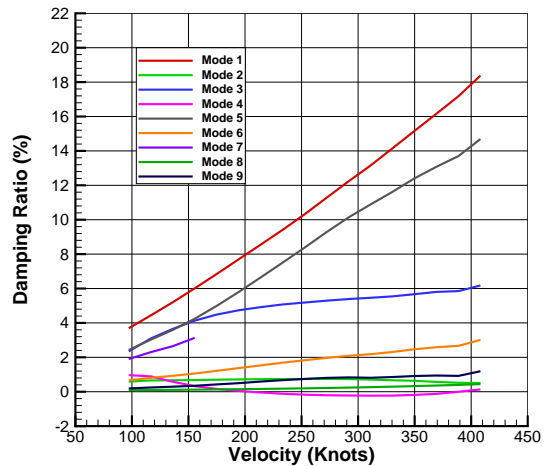


Figure 14: 15% Pylon Stiffness Damping Ratios with Wing Aerodynamics

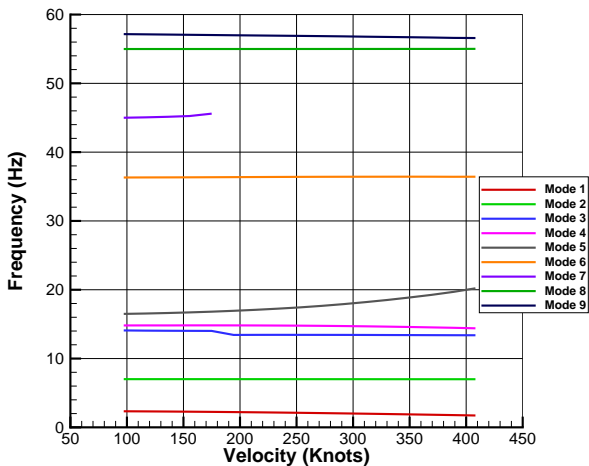


Figure 15: 12% Pylon Stiffness Frequencies with Wing Aerodynamics

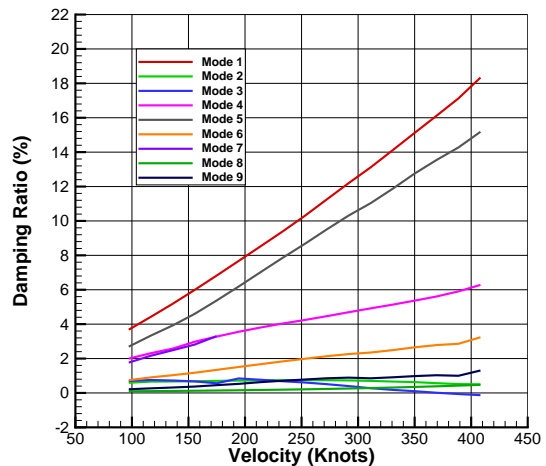


Figure 16: 12% Pylon Stiffness Damping Ratios with Wing Aerodynamics

Figures 11 through 16 show the frequencies and damping ratios of the semi-span system with the additional damping of wing aerodynamics. Across the range of weakened pylon stiffness the frequencies remain unchanged with the exception of modes 3 and 4. This is due to the two modes becoming uncoupled as a result of the weakened pylon spring stiffness. The damping ratios tell a different story. An 18% stiff pylon yields a marginally stable system at low speeds but becomes more stable as the flight speed is increased. When reducing the pylon stiffness by 3%, a disparity arises. Here the fourth mode becomes unstable, and remains unstable for the vast majority of the flight regime (Fig.14). Decreasing the pylon spring stiffness by another 3% shows, yet again, a contrast in the results detailed in Figure 14, for a 15% stiff pylon spring. Figure 16 shows that the system is stable until a flight speed of 350 knots. Here, the third mode becomes unstable, and the fourth mode is very stable.

3.3 Non-Rotating Propeller

This section shows that it is the spinning propeller that drives the instability and not the coupling of wing modes. The propeller/pylon system is still present but contributes no airloads or gyroscopic forces. Even though the two second out-of-plane bending modes are close for the baseline propeller whirl flutter, the system is stable.

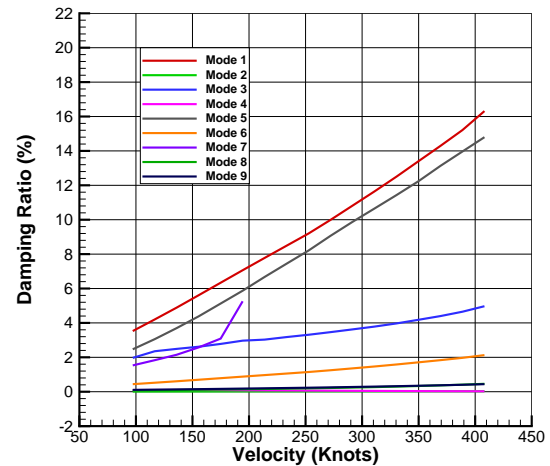
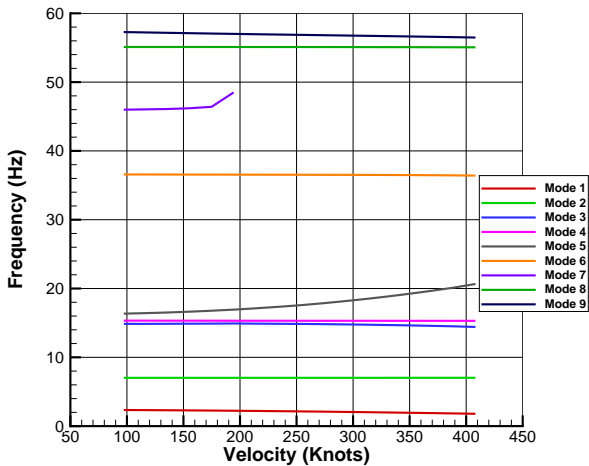


Figure 17: Non-Rotating, 15% Stiffness Frequencies Figure 18: Non-Rotating, 15% Stiffness Damping Ratios

3.4 Velocity Reduction

In this section, the free stream velocity is reduced to observe the impact on stability. Figures 19 through 22 show the frequency and damping ratios of a velocity reduction to 80% and 50% of the free stream velocity at five seconds. The significance of this time stamp is that the system has been perturbed, whirl flutter has begun, and the velocity reduction has taken place. The x-axis for the figures in this section show the initial velocities before the decrease in speed in order to compare with the baseline. Since an instantaneous deceleration isn't realizable, a body force with an acceleration corresponding with the slow down of the vehicle over two seconds is applied. This acceleration becomes large at the higher velocities, equating to two G's of acceleration for the 80% case and five G's for the 50% case. It can be seen that the decrease in speed down to 80% of the current velocity that the speed reduction can cause the instability to dampen out and the system to become stable. However, when the speed reduction is too quick and involves a large acceleration, the system can become more unstable and previous velocities become unstable. For the 50% case, it is the second mode or the in-plane bending mode that becomes unstable due to the large acceleration. As with the baseline, the mode identification begins to break down after the system is unstable.

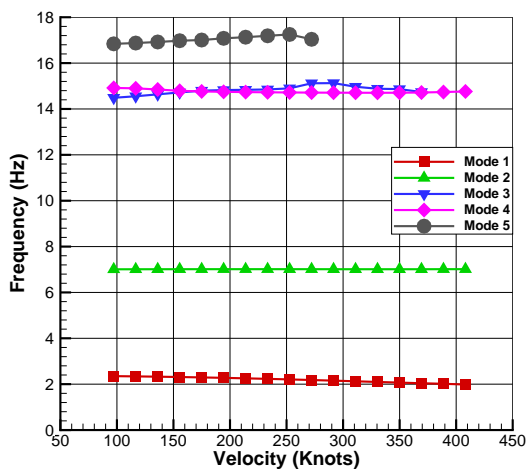


Figure 19: Frequencies Versus 80% Velocity Reduction

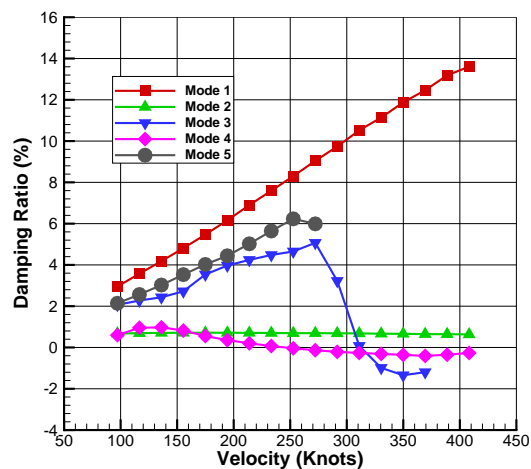


Figure 20: Damping Ratios Versus 80% Velocity Reduction

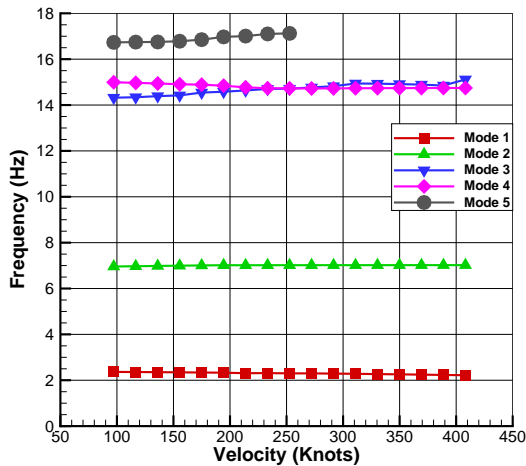


Figure 21: Frequencies Versus 50% Velocity Reduction

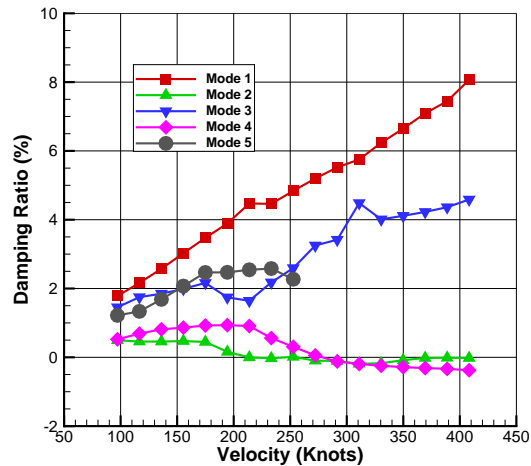


Figure 22: Damping Ratios Versus 50% Velocity Reduction

3.5 Propeller RPM Change

This section will detail the response of the pylon pitch and yaw responses with a reduced RPM of the tip propeller. The pylon spring stiffness will be assumed to already be damaged, meaning that the spring will be 15% of the nominal stiffness. The reduced RPM will be assumed to have already happened and the perturbation of the gust will be applied in the same manner as the other testing scenarios. The establishment of a baseline for comparison is made in the following figure. Furthermore, wing aerodynamics are neglected to measure the motion of pylon pitch and yaw without any additional stabilizing aerodynamics. A baseline case using the cruise condition for the main drive rotors of 2250 RPM at 8,000 ft is made to compare the response with a percentage of RPM from the stated cruise condition. In the baseline case, the system is stable using 100% of the cruise RPM (Fig.5). Reducing the RPM to 90% of the nominal value yields very similar results in the first and third modes. However, the remaining three modes see a similar trend with respect to increasing velocity, but at a lower damping ratio.

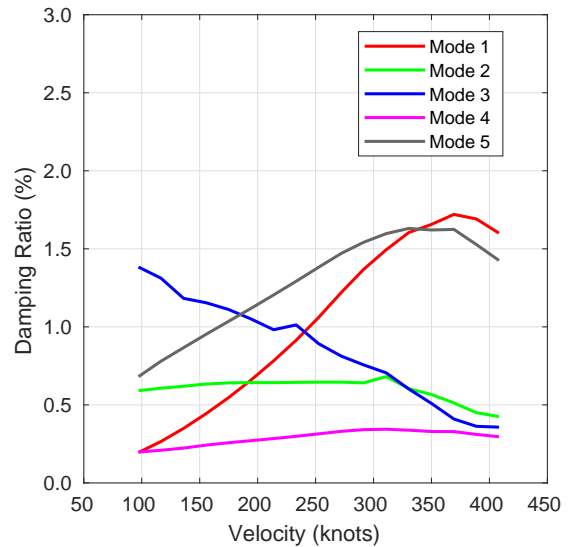
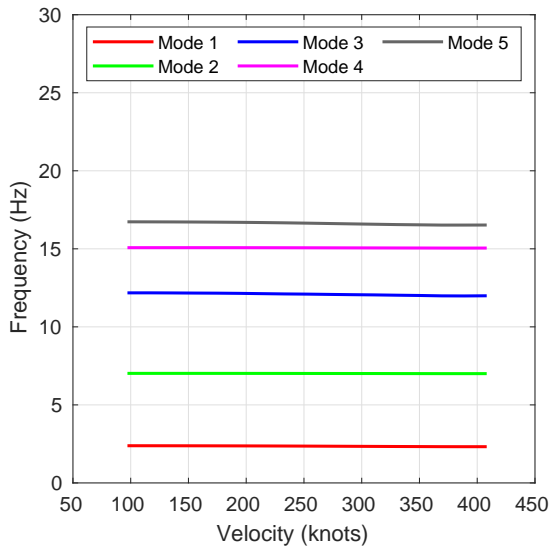


Figure 23: 90% RPM Reduction Frequency and Damping Ratios

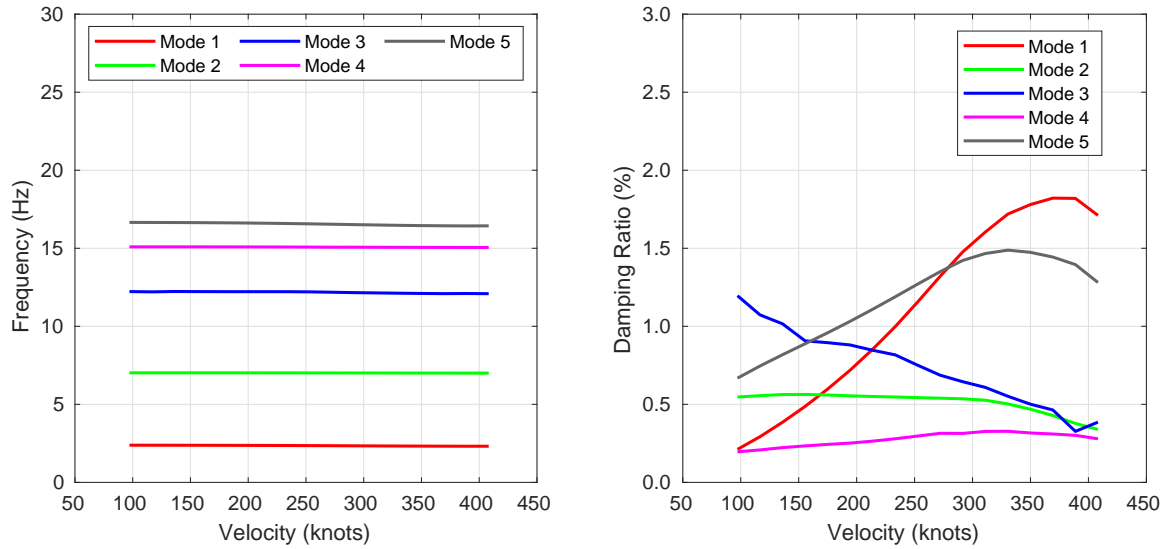


Figure 24: 81% RPM Reduction Frequency and Damping Ratios

The exclusion of wing aerodynamics gives a stable system for the damaged pylon stiffness simulated. Reducing the RPM from the nominal cruise condition does not change the response seen in mode 1. Mode 2 sees a reduction in damping with decreasing RPM, and the same is seen in the response for mode 5. Modes 3 and 4 are pylon pitch and pylon yaw. Both of these modes are stable without wing aerodynamics acting on the model. The addition of wing aerodynamics does cause the fourth mode to be unstable in Figure 14, with the nominal condition for cruise RPM. The reduction of the RPM shows progressive improvement until 75% of the cruise RPM is reached, and the critical fourth mode becomes stable (Fig.27). The system becomes more stable with the reduction of the RPM to 66% of the nominal cruise RPM.

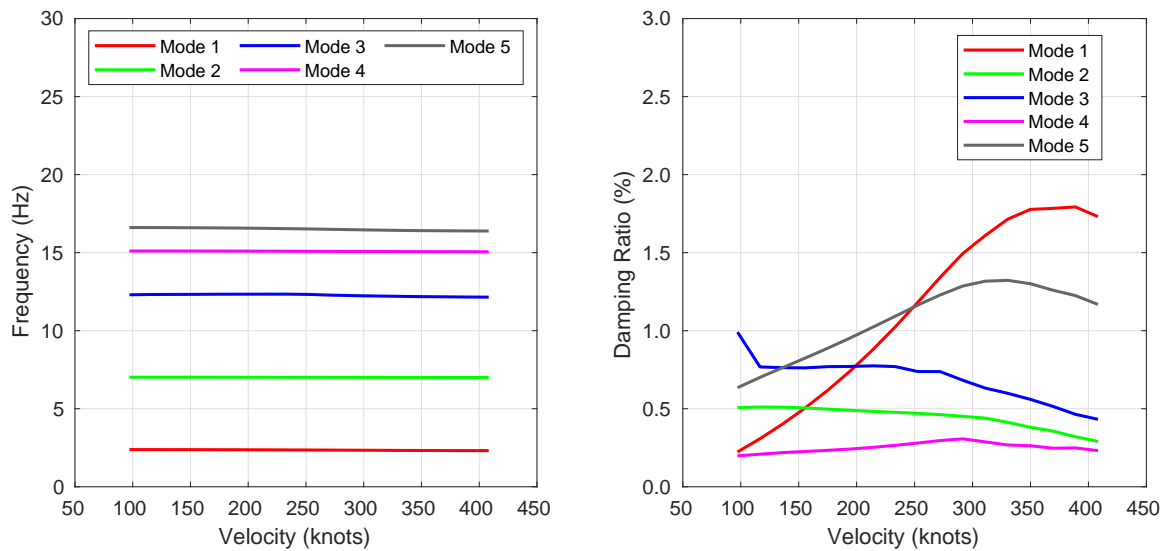


Figure 25: 75% RPM Reduction Frequency and Damping Ratios

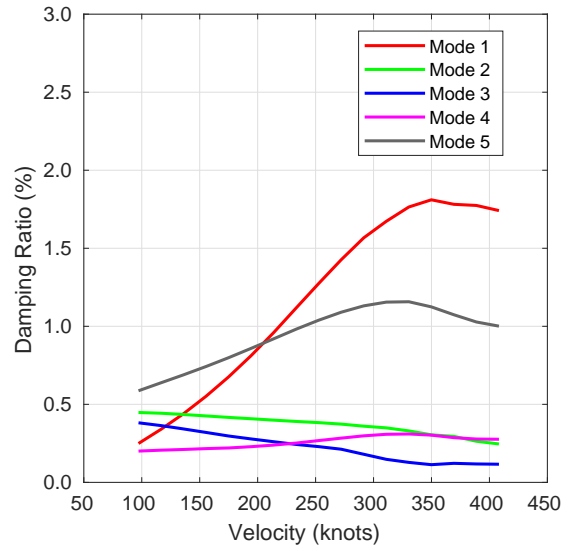
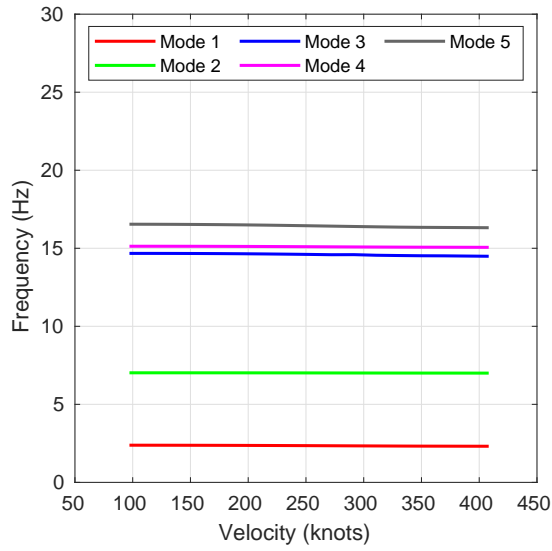


Figure 26: 66% RPM Reduction Frequency and Damping Ratios

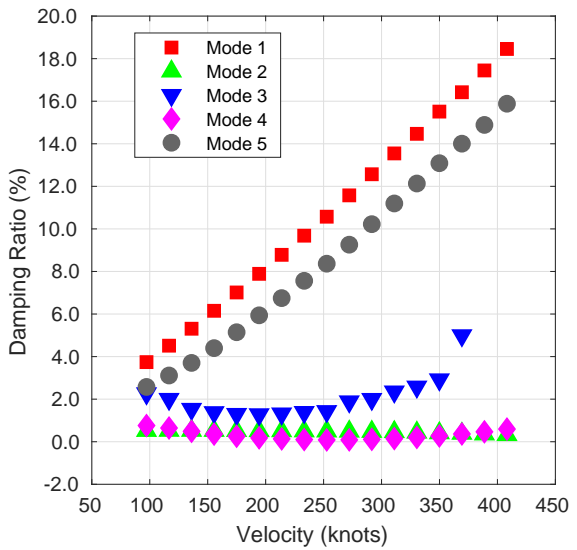
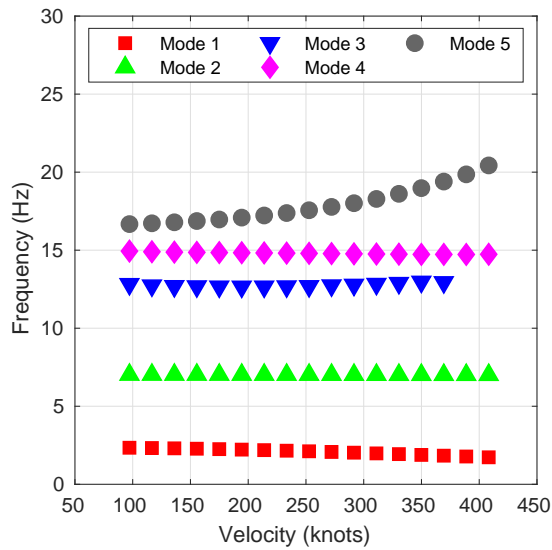


Figure 27: 75% RPM Reduction Frequency and Damping Ratios with Wing Aerodynamics

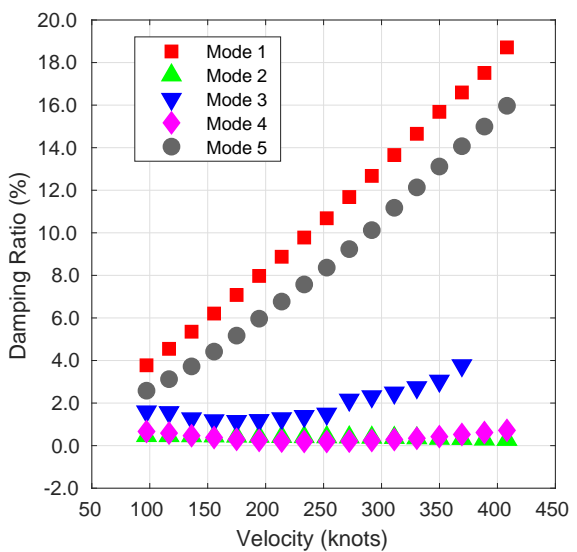
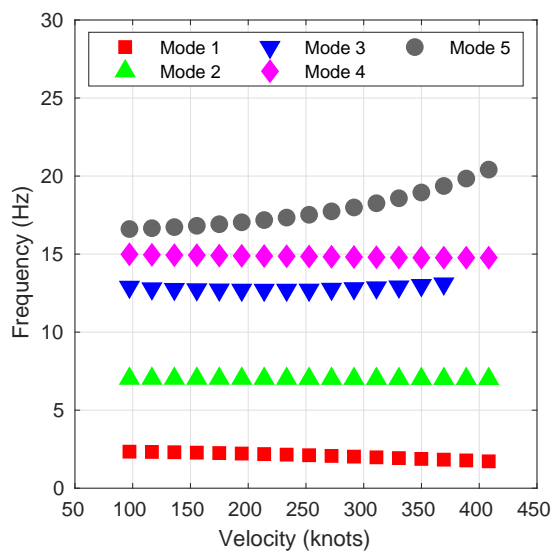


Figure 28: 66% RPM Reduction Frequency and Damping Ratios with Wing Aerodynamics

3.6 Propeller Pitch Change

Up to now, the results presented in this paper have considered a range of velocities for the rotor spinning at windmilling conditions. A second mitigation technique that the pilot can use to control or reduce the effect of whirl flutter is changing the rotor angle of pitch. This section will study the effect of rotor pitch angle on whirl flutter for two different rotor RPM settings and altitudes, as well as taking into consideration the effect of wing aerodynamics. The altitudes tested are sea level and 8,000 feet. These are the take off and cruise altitudes.

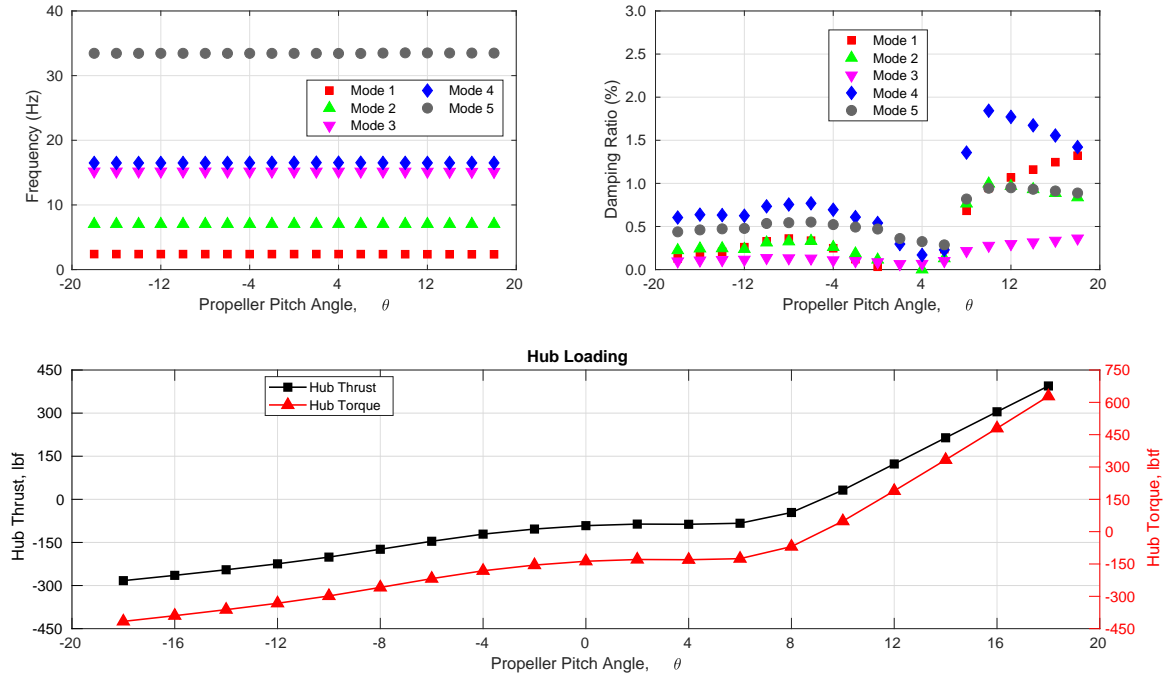


Figure 29: Pitch Change Response with X-57 Airfoil at Sea Level

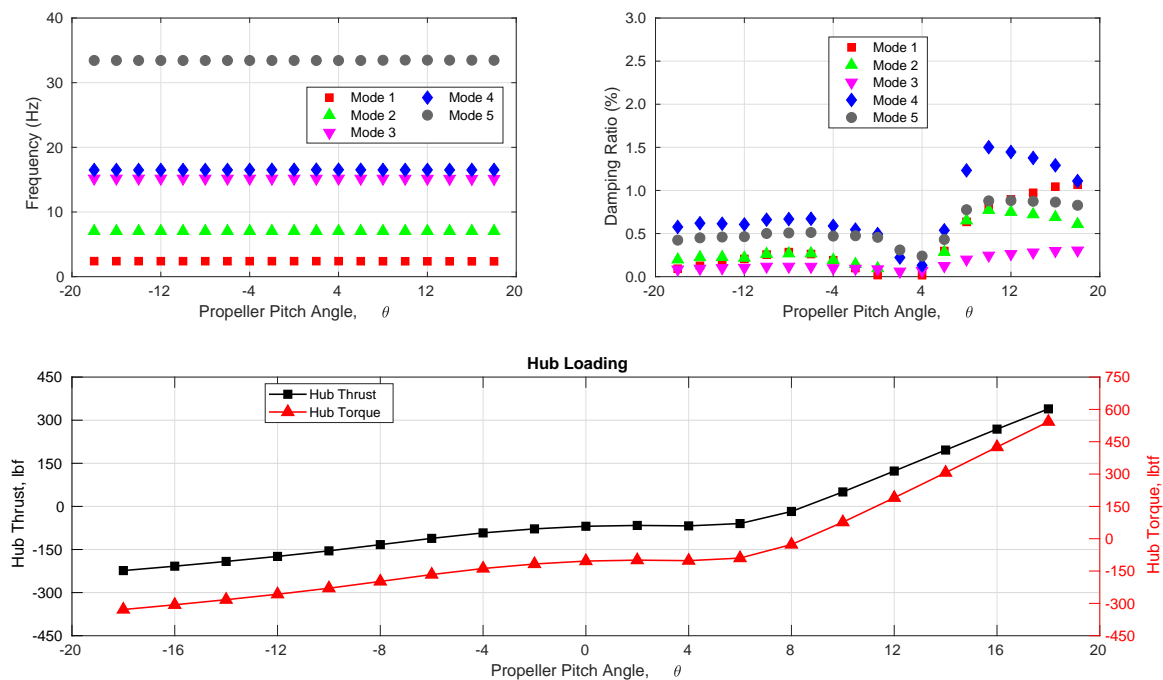


Figure 30: Pitch Change Response with X-57 Airfoil at 8,000 ft

The flight velocity chosen for the pitch change is 213 knots. This flight velocity is significant because it is the first velocity that is unstable when the pylon stiffness is reduced to 15% of the nominal value. Pylon stiffness is at the nominal value in these simulations; however, the system can go unstable as seen in Figure 29. At the cruise altitude, the system is unstable in with the pitch angle ranging from 0° to 4°. The thrust and torque in this region is negative as shown in either Figure 29 or 30.

3.6.1 NACA 0012 Airfoil Results

With consistent frequencies for the airfoils designed for this aircraft, but inconsistent damping ratio values across the range of pitch angle, a study with a NACA 0012 airfoil was conducted in the same fashion.

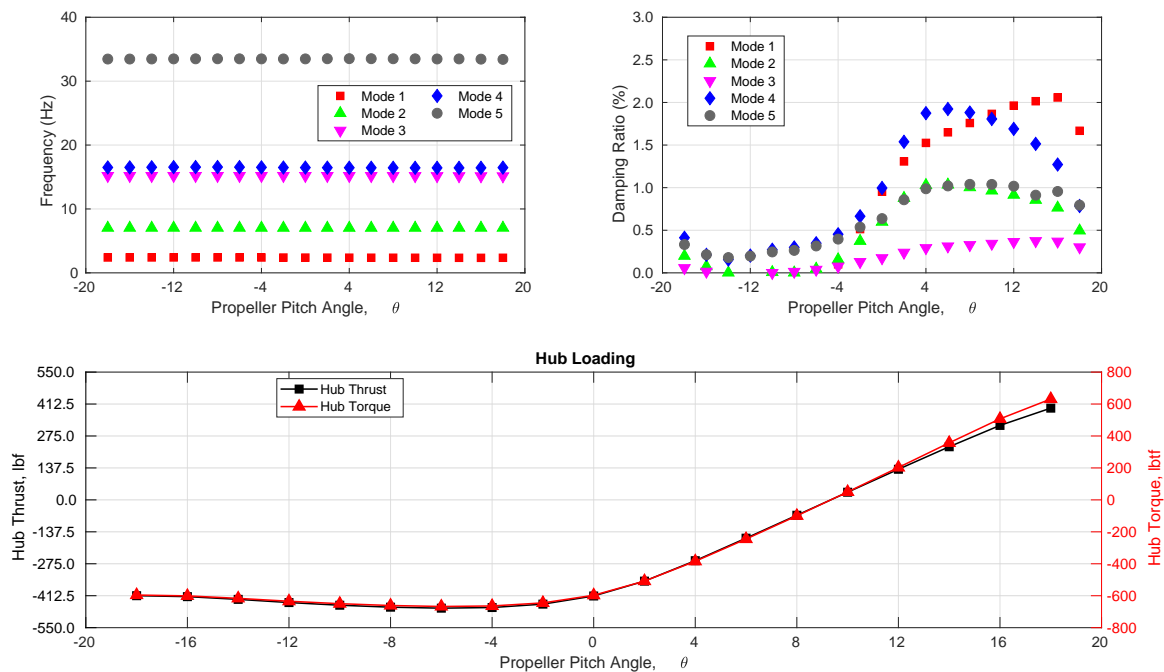


Figure 31: Pitch Change Response with NACA 0012 Airfoil at Sea Level

The NACA 0012 airfoil is widely utilized and is used in this study as a validation measure for the X-57 airfoil. The results here are comparable to the the results using the X-57 airfoils. Despite the unique airfoil design for the X-57 that embodies the rotor blade tested in Figures 29 and 30, Figures 31 and 32 show similar trends in damping using a NACA 0012 airfoil. The frequencies seen between the two airfoil designs are also comparable. Without wing aerodynamics, the system is unstable when the airfoils are in the stall region around -16° of pitch angle.

3.6.2 Effect of Density

A brief case study was done to see what affect that density would have on the wing frequencies and damping ratios. Another change that is made for this study is different RPM. The cruise RPM of 2250 RPM and the take-off RPM of 2700 RPM will be used at both altitudes. Figures 33 and 34 show the results of the take-off and cruise altitudes frequency and damping ratios with a propeller at 2250 RPM and 2700 RPM, respectively. Wing aerodynamics plays little part in the frequency seen between the altitudes for both RPM sets. The damping ratio, on the other hand, heavily depends on the addition of wing aerodynamics as previously seen in this paper. For both RPM cases depicted, the change in density does effect the damping ratios of the system. Operating at a lower altitude, increases the damping ratios most dramatically in

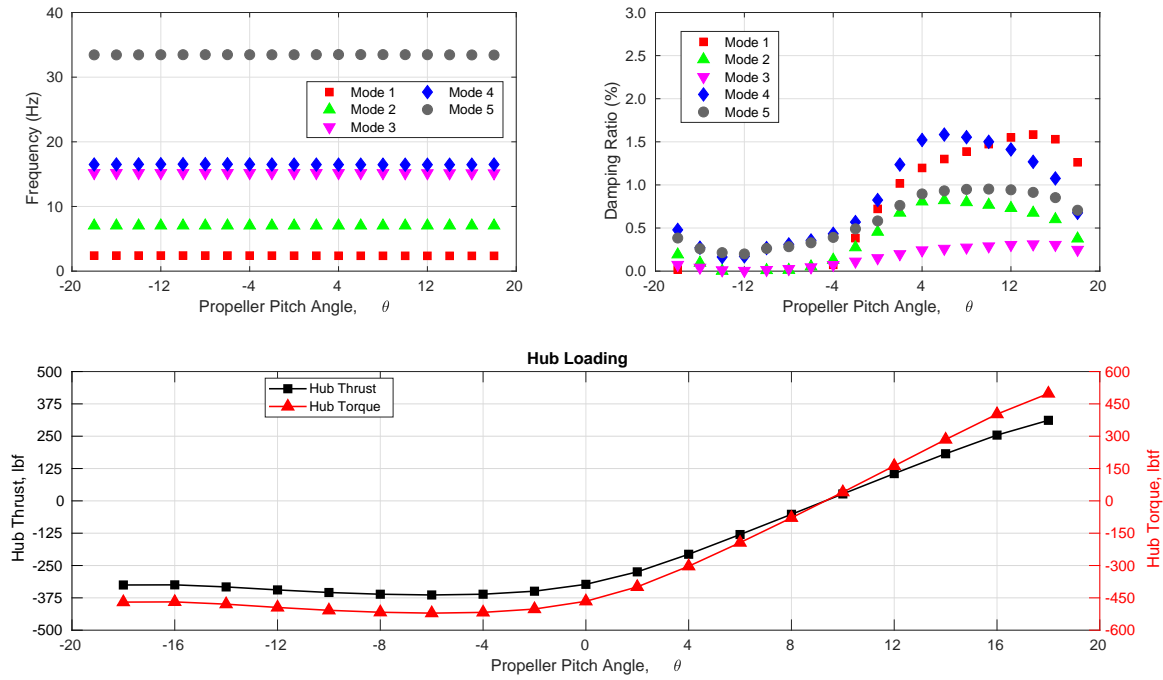


Figure 32: Pitch Change Response with NACA 0012 Airfoil at 8,000 ft

mode 4. In the entire range of propeller pitch angle, modes 3 and 5 give a negligible change in damping between sea level and 8,000 ft. Modes 1 and 2, on the other hand, show that the lower altitude case have higher damping with propeller pitch angle greater than 4° . Unfortunately, with an undamaged pylon, the system can still become unstable with the second mode going unstable with a pitch angle ranging from 0° to 4° (Fig. 33). These pitch angle range generates negative thrust, thus outside the normal operation range.

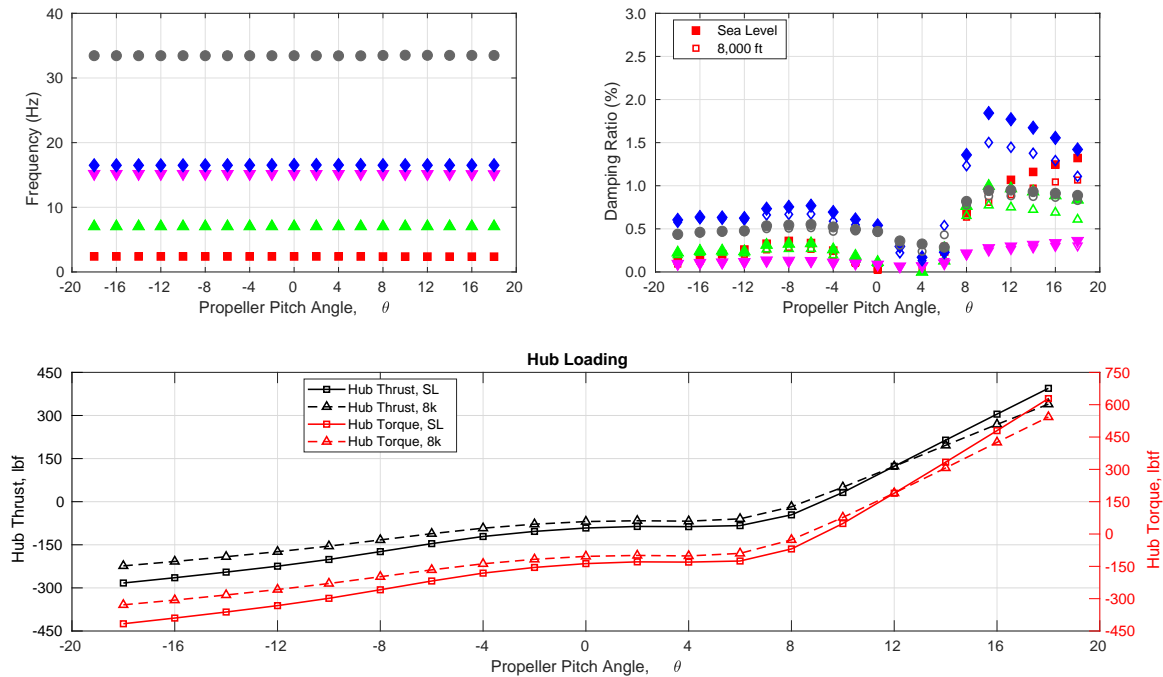


Figure 33: Altitude comparison at 2250 rpm

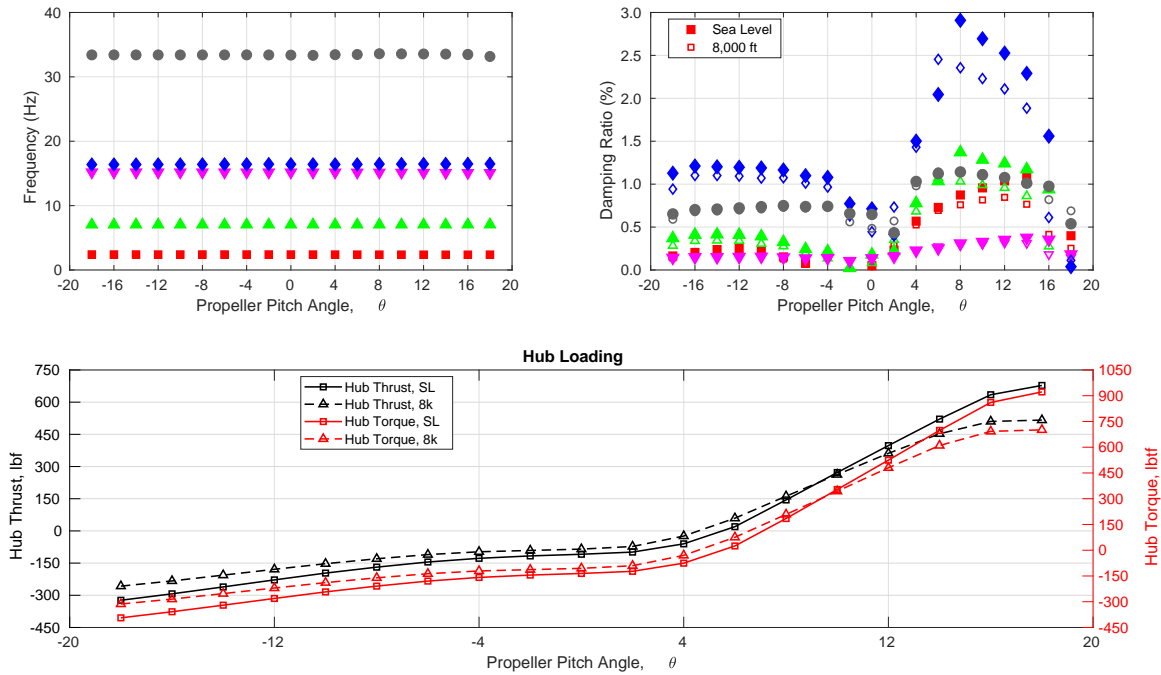


Figure 34: Altitude comparison at 2700 rpm

4 SUMMARY AND CONCLUSIONS

This paper has presented a parametric study, which analyzed the effect of a weakened pylon stiffness and the response after a gust of wind perturbed the system. The results here found that a damaged pylon equal to 15% of the nominal pylon stiffness causes a coupling of the elastic wing mode and short period mode to be unstable. This decoupled mode saw the second out of plane bending in pylon yaw to become unstable. Furthermore, this paper introduced a few mitigation methods to give the pilot instruction so that, when whirl flutter occurs, the chance of controlling the effect or reversing the vibration can be achieved. A reduction in RPM had little effect if reducing the velocity to 90%, but reducing the RPM to 81% and lower will stabilize the system. Another mitigation method tested and presented in this paper is changing the pitch of the propeller blades. The results show that, without wing aerodynamics, the system is stable for the positive thrust region of the airfoil being used in this aircraft. A comparative study using a NACA 0012 airfoil was used, so that the standardized, widely used airfoil can be used as a benchmark. In both cases, the pylon pitch and pylon yaw motions are unstable in the same region of propeller pitch, from 0° to 4° of propeller pitch angle, where the thrust is negative.

Finally, a study was conducted on the effect of air density on whirl flutter. Sea level and 8,000 feet were simulated. Instability follows the same trend as the pitch change results, where the density change lowered the damping ratios slightly.

5 ACKNOWLEDGMENTS

The study was funded by NASA Langley Research Center through National Institute of Aerospace. The authors would like to thank Jennifer Heeg(NASA Langley Research Center) for her support for this study, and Olivier Bauchau (University of Maryland, College Park) for providing the Dymore analysis.

6 REFERENCES

- [1] Borer, N. K., Patterson, M. D., Viken, J. K., et al. (2016). Design and performance of the nasa sceptor distributed electric propulsion flight demonstrator. 16th AIAA Aviation Technology, Integration, and Operations Conference.
- [2] Dubois, A., van der Geest, M., Bevirt, J., et al. (2016). Design of an electric propulsion system for SCEPTOR’s outboard nacelle. In *16th AIAA Aviation Technology, Integration, and Operations Conference*. American Institute of Aeronautics and Astronautics. doi: 10.2514/6.2016-3925.
- [3] Patterson, M. D. and Borer, N. K. (2017). Approach considerations in aircraft with high-lift propeller systems. 16th AIAA Aviation Technology, Integration, and Operations Conference.
- [4] Heeg, J. and Stanford, B. K. (2019). Whirl flutter and the development of the nasa x-57 maxwell. In *International Forum on Aeroelasticity and Structural Dynamics*. Hampton, VA.
- [5] Taylor, E. S. and Browne, K. A. (1938). Vibration isolation of aircraft power plants. *Aero Sci* 6, no. 2, 43.
- [6] Abbott, F. T., Kelly, H., and Hampton, K. D. (1963). Investigation of propeller-power-plant autoprecession boundaries for a dynamic-aeroelastic model of a four-engine transport airplane. NASA tech. Note D-1806.
- [7] Houbolt, J. C. and Reed III, W. H. (1961). Propeller-nacelle whirl flutter. IAS 29th Annual Meeting.
- [8] Bauchau, O., Bottasso, C., and Nikishkov, Y. (2001). Modeling rotorcraft dynamics with finite element multibody procedures. *Mathematical and Computer Modeling*, 33, 1113–1137.
- [9] Hoover, C. B., Shen, J., Kreshock, A. R., et al. (2017). Whirl flutter stability and its influence on the design of the distributed electric propeller aircraft x-57. In *17th AIAA Aviation Technology, Integration, and Operations Conference*. Denver, CO: American Institute of Aeronautics and Astronautics. doi:10.2514/6.2017-3785.
- [10] Hoover, C. B. and Shen, J. (2018). Parametric study of whirl flutter stability of the NASA aircraft x-57. In *2018 AIAA Aerospace Sciences Meeting*. American Institute of Aeronautics and Astronautics. doi:10.2514/6.2018-0276.
- [11] Peters, D. and He, C. (1995). Finite state induced flow models. part i: Two dimensional thin airfoil. *Aircraft*, 32(2), 313–322.
- [12] Bauchau, O. A. (2016). *DYMORE USERS MANUAL*.
- [13] Weiss, L. and McDonough, R. N. (1963). Prony’s method, z-transforms, and padé approximation. *SIAM Review*, 5(2), 145–149. doi:10.1137/1005035.